J. Chem. Sci. Vol. 127, No. 8, August 2015, pp. 1435–1450.
DOI 10.1007/s12039-015-0914-y

Structural and vibrational spectral studies on hydrogen bonded salts: 4-chloroanilinium maleate and nitrate

R ANITHA[a], M GUNASEKARAN[a], S SURESH KUMAR[b] and S ATHIMOOLAM[b,*]

[a]Department of Physics, Regional Centre, Anna University Tirunelveli Region, Tirunelveli 627 007, India
[b]Department of Physics, University College of Engineering, Nagercoil, Anna University, Nagercoil 629 004, India
e-mail: athi81s@yahoo.co.in

MS received 25 October 2014; revised 17 May 2015; accepted 19 May 2015

Abstract. In the present study, proton transfer from nitric and maleic acids to amine group (4-chloroaniline) led to hydrogen bonded crystals of 4-chloroanilinium maleate (4CAM) and 4-chloroanilinium nitrate (4CAN) which are investigated by the experimental and theoretical approaches. The molecular structures of these two compounds were optimized with the Density Functional Theory (DFT) using B3LYP function and the Hartree-Fock (HF) level with a6-311++G(d,p) basis set. Geometrical parameters of the molecules were also analyzed along with their intermolecular hydrogen bond, which tailors the ions. These analyses show that present molecules are stabilized through the N–H$\cdots$O and O–H$\cdots$O hydrogen bonds. The vibrational modes were computed by quantum chemical methods. Further, these modes are investigated by FT-IR and FT-Raman spectroscopy in the range of 4000–400 cm^{-1}. The optimized molecular geometry and computed vibrational spectra are compared with experimental results, which show significant agreement. The natural bond orbital (NBO) analysis was carried out to interpret hyperconjucative interaction and intramolecular charge transfer (ICT). This analysis gives the precise insight into the nature of H-bond interactions. The chemical hardness, electronegativity and chemical potential of the molecules were determined by HOMO–LUMO plot. The frontier molecular orbitals have small band gap value, which signify the possible biological/pharmaceutical activity of the compounds.

Keywords. FT-IR spectrum; FT-Raman spectrum; Vibrational analysis; quantum chemical analysis; HOMO–LUMO; NBO.

1. Introduction

One of the most important reactions in chemistry and biochemistry is proton transfer between donor and acceptor.[1] These interactions are playing an important role in various chemical and biological processes such as stabilizing the biomolecular structures,[2] controlling the speed of the enzymatic reactions[3] and constructing supramolecular structures.[4] In most of the cases, the applications are ensued due to the intra- and intermolecular interactions particularly with the hydrogen bonds, which have more importance in the areas of molecular recognition, crystal engineering research and supramolecular chemistry. Understanding of these non-covalent interactions has proved to be the most valuable because of its strength and directional properties.[5] The strength and directionality of hydrogen bonding interactions are responsible for solid-state formation and other physical properties of the system.[6] Also, we continuously seek to identify hydrogen bond–enriched assemblies by means of efficient organic hydrogen bonding synthons.

Substituted anilines are known to be candidates for supramolecular synthons as they have both donor and acceptor sites, viz., nitrogen and chlorine atoms in the present case. The present work was attempted with nitrate and maleate salts of 4-chloroanilinium crystal. Though the single-crystal XRD clearly predicts the molecular structure and packing tendency of the molecule in the solid crystalline state, the spectral measurement gives an account of the strength of the intermolecular interactions by means of shifting of wavenumbers and the intensity of the peaks. Further, the molecular geometry obtained from the crystallographic data is a well-suited input for the quantum chemical calculations. By which it is possible to optimize the molecule in different environments and the corresponding vibrational modes can be calculated. The hyperconjugative interactions and band gap values can be inferred from natural bond orbitals (NBOs) and frontier molecular orbital (FMO) studies. Hence, a combined crystallographic, spectroscopic and quantum chemical calculations were

*For correspondence

attempted on 4-chloroanilinium maleate (4CAM) and 4-chloroanilinium nitrate (4CAN), and the results are summarized.

2. Experimental

2.1 *Crystal Growth*

Crystals of 4CAM and 4CAN were synthesized from aqueous mixtures containing 4-chloroaniline with maleic and nitric acid in the 1:1 stoichiometric ratio at room temperature by slow evaporation method, respectively. After a week, light yellow colour crystals of 4CAM and 4CAN were obtained. The qualities of the crystals were improved by recrystallization.

2.2 *Density Measurement*

The density of the grown crystals were measured by sink and swim method (flotation technique) using a liquid mixture of carbon tetrachloride and xylene. Initially, carbon tetrachloride (5 mL) was taken in a test tube and a good-quality three-dimensional crystal was placed on it. Due to high density of the liquid, the crystal began to float. Then, drops of xylene were added drop by drop with continuous agitation to get uniform density over the liquid. When the density of the crystal matches that of liquid mixture, the crystal levitates to the middle of the test tube. Then, the density of the liquid was found with specific gravity bottle from the concept of relative density. Thus, the densities of the crystals are found to be 1.495 $mg.m^{-3}$ for 4CAM and 1.465 $mg.m^{-3}$ for 4CAN.

2.3 *Single-Crystal XRD Studies*

The entire crystallographic calculations of 4CAM were performed done using single-crystal X-ray diffraction by Bruker SMART APEX CCD area detector diffractometer (graphite- monochromated, $MoK_{\alpha} = 0.71073$ Å). A good-quality single-crystal was selected from the grown crystals and used for the single crystal X-ray diffraction studies. Consequently, the full data collection of the crystal was carried out. The cell refinement and data reduction were done with XCAD4 software.[7] The structure was solved and refined with the SHELXL97 program.[8] All the H atoms were discernible in the difference electron density maps. Nevertheless, the aryl H atoms were constrained and refined in the riding atom approximation: C−H = 0.93,Å and $U_{iso}(H) = 1.2U_{eq}(C)$. The other H atoms, which are involved in the N−H···O and O–H...O hydrogen bonds, were located from electronic density map and refined isotropically. Graphical molecular illustrations were done with ORTEP3 for Windows[9] and Mercury[10] packages.

Though good-quality crystals of 4CAN were obtained, the attempts of single crystal X-ray diffraction was not fruitful due to the hygroscopic nature of the crystal.

2.4 *Vibrational Spectroscopic Measurements*

A Jasco spectrometer FT-IR, model 410 under a resolution of 4 cm^{-1} and with a scanning speed of 2 mm/sec was used for IR spectral measurements. The samples were prepared using pellet technique and the spectrum was recorded over the range 4000–400 cm^{-1}. The FT-Raman spectrum was recorded in the frequency range of 4000–50 cm^{-1} using a BRUKER RFS 27 FT-Raman Microscope module with the resolution of 2 cm^{-1}. The Nd: YAG Laser source was operated at 1064 nm for the excitation.

2.5 *Computational details*

The geometrical optimization for 4CAM and 4CAN molecules was carried out theoretically by 6-311++ G(d,p) level on an Intel Core i5/3.20 GHz computer using Gaussian 09W[11] program package without any constraint.[12] Initial geometry was taken from the single-crystal X-ray studies and it was minimized (optimized) by Hartree−Fock (HF) method using the 6-311++G (d,p) basis set. The molecular geometries were also optimized by the Density Functional Theory (DFT) using the Becke's three-parameters exchange functional (B3)[13] in combination with the Lee–Yang–Parr correlation functional (LYP).[14] It is accepted as a cost-effective approach for the computation of molecular structure, vibrational frequencies and energies of optimized structures. The optimized structural parameters were used in the vibrational frequency calculations at the same level to characterize all stationary points as minima. Then vibrationally averaged nuclear positions of the structure were used for harmonic vibrational frequency calculations resulting in IR and Raman frequencies. Finally, the calculated normal mode vibrational frequencies provide thermodynamic properties through the principle of statistical mechanics. By combining the analysis preformed using the GAUSSVIEW program[15] with symmetry considerations, vibrational frequency assignments were made with a high degree of accuracy. There is always some ambiguity in defining internal coordination. However, the defined coordinate from the complete set matches quite well with the motions observed using the GAUSSVIEW program. Also, the NBO calculations were carried out using HF and DFT methods

with the 6-311++G (d,p) basis set to get more detailed information about the chemical bonds and hydrogen bonding interaction within the ions. The FMOs have been computed and analyzed by HF and DFT method with the 6-311++G (d,p) basis set.

3. Results and Discussions

3.1 *Molecular Geometry*

The solid-state molecular and crystal structures of 4CAM are illustrated from the single-crystal XRD studies. The asymmetric part of the 4CAM contains a 4-chloroanilinium cation and a maleate anion shown in figure 1. As 4CAN is prepared with 4-chloroaniline and nitric acid, the crystals are expected to possess 4-chloroanilinium cation and a nitrate anion in the asymmetric part. The optimized structures of both the molecular assemblies are shown in figure 2. In both the compounds, the transfer of proton from the inorganic and organic acid leads to protonation on the NH_2 sites of the 4-chloroaniline and it forms the 4-chloroanilinium cation. This protonation on the N site of the cation is confirmed from the elongated C−N bond distance [1.456 (3) Å] in 4CAM.[16] The protonated bond distance is compared with the theoretically computed bond distances. The optimized C–N bond distances are 1.418 and 1.426Å in HF and DFT levels, respectively, for 4CAN and 1.415 and 1.425 Å by the HF and DFT levels, respectively, for 4CAM (table 1). In theoretical calculations the C–N bond distances of the molecules are observed to be smaller than the single crystal XRD study which is due to the effect of N–H···O intermolecular hydrogen bonds. Even though the hydrogen atom seems to have deviated from the N atom of the cation, there must be some attraction between cation and anion which is confirmed by the Mulliken charge distribution analysis. The bond geometry between N, H and O atoms which connect the ion pairs, are shown scheme 1. From the Mulliken charge distribution analysis of the two complexes, N atom is more electronegative than the O atom. These N atoms of the cations are attracting the proton from acids and it forms the N–H···O intermolecular hydrogen bond. The N–H···O angle is 180° and 179° at the HF and DFT/B3LYP methods, respectively, for 4CAN and 172° in both methods for 4CAM, whereas the experimental counterpart is only 158 (2)°. Hence, this intermolecular hydrogen bonding effect is perceived to be dominant in the DFT/B3LYP and HF methods than in the experimental methods.

In 4CAM, the planes of the cation and maleate anion are inclined at an angle 15.6 (1)° in the single crystal

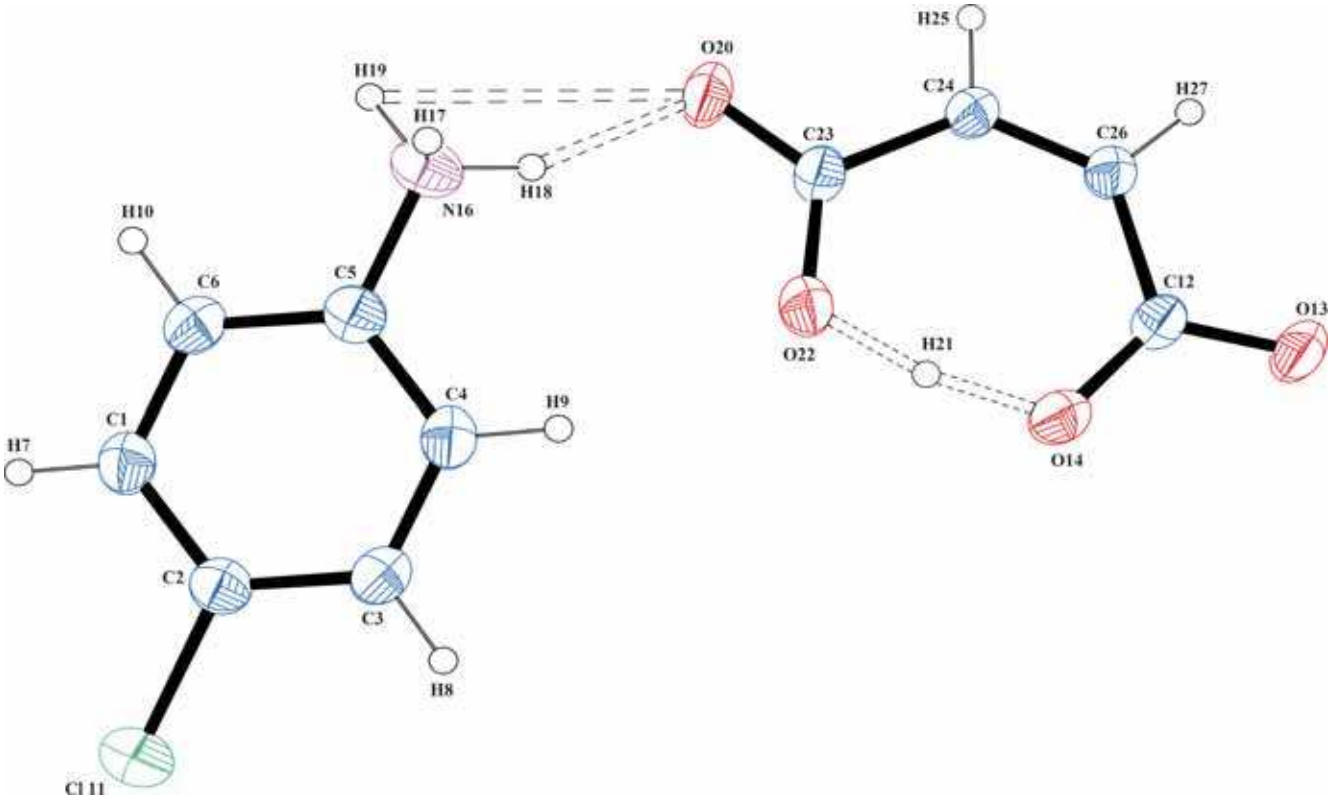

Figure 1. The molecular structure of the 4CAM with the numbering scheme for the atoms and 50% probability displacement ellipsoids.

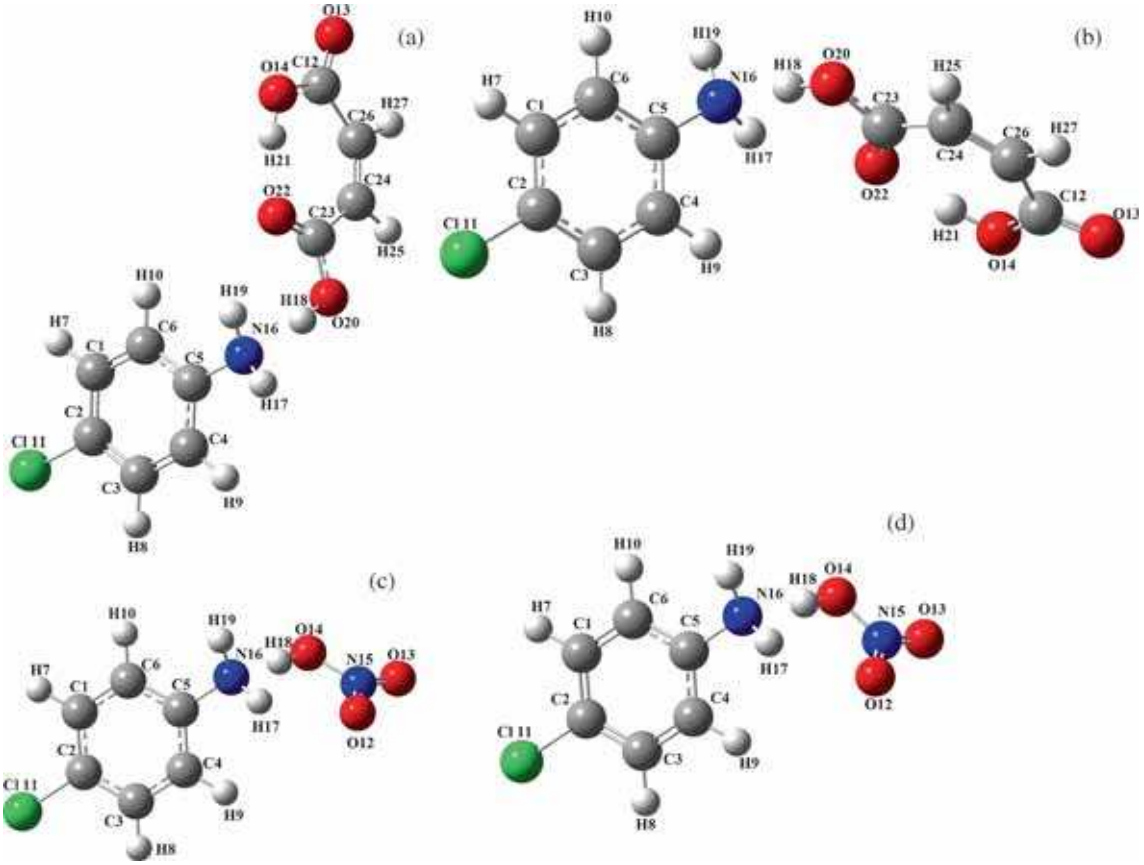

Figure 2. Optimized molecular geometry and atomic numbering scheme by HF (a) DFT; (b) methods for 4CAM and HF; (c) DFT; (d) for 4CAN.

XRD, these planar angles are calculated at 73.6° and 73.9° in HF and DFT methods respectively. These deviations occur due to the reorientation of N–H$\cdots$O intermolecular hydrogen bond. The C–O bond distances of the carboxylate group from the maleate anion are 1.182–1.302 Å at the HF level and 1.209–1.330 Å by the B3LYP method, whereas in experimental methods it is 1.234 (2)–1.267 (2) Å (table 2). The planarity of the maleate anion is confirmed by the torsion angles.

In 4CAN, the nitrate group exists in a planar orientation with the O–N–O angles varying from 115.5 to 127.6° in HF level and from 115.1 to 128° in the DFT/B3LYP method. The average bond lengths varied at 1.189–1.318 and 1.222–1.379 Å in the HF and DFT/B3LYP methods respectively (table 3). One of the N–O bond distances (1.318 Å in HF and 1.379 Å in B3LYP) in the nitrate anion increases more than the literature value ($\sim$1.240 Å). This elongation is due to the N–H$\cdots$O hydrogen bond between the cation and anion. It shows the possible charge transfer between donor N and acceptor O atoms. This hydrogen bonding effect is less in the HF level, which is revealed in the computed spectra. The $-NH_2$ stretching mode of NH_3^+ group is observed to be low-intense peak in the HF level, whereas it is the strongest among the computed vibrational peaks in the DFT/B3LYP level.

The optimized C–C bond lengths of phenyl ring are in the falling range 1.381$-$1.392 Å, according in the theoretical calculations, whereas the single-crystal XRD reveals the C–C bond lengths in the range of 1.368–1.376 Å. On comparison, it is observed that most of the optimized bond lengths are slightly deviated from the experimental values. Because theoretical calculations were carried out for the molecules in the free gaseous phase and the experimental results corresponding to the molecules are in the solid crystalline state.

3.2 *Mulliken Charge Analysis*

In general, Mulliken atomic charge calculation has an important application of quantum chemical calculations to molecular systems. It plays a vital role in the packing of crystals in the solid state by means of intermolecular interaction and it has significant influence on dipole moment, polarizability, electronic structure and vibrational modes.[17] The Mulliken charge analyses of molecules 4CAM and 4CAN are calculated at the HF and DFT/

Table 1. Comparison of optimized molecular geometrical parameters of 4-chloroanilinium cation.

Atom	4CAN		4CAM		
Connected	HF	DFT	HF	DFT	Experimental[#]
Bond length (Å)					
C1-C2	1.381	1.391	1.381	1.391	1.370 (2)
C1-C6	1.384	1.392	1.384	1.392	1.373 (2)
C1-H7	1.074	1.082	1.074	1.082	0.930
C2-C3	1.381	1.391	1.381	1.391	1.368 (2)
C2-CL11	1.745	1.758	1.745	1.758	1.728 (2)
C3-C4	1.383	1.392	1.384	1.392	1.373 (2)
C3-H8	1.074	1.082	1.074	1.082	0.930
C4-C5	1.388	1.397	1.388	1.397	1.363 (19)
C4-H9	1.076	1.085	1.076	1.085	0.930
C5-C6	1.387	1.397	1.388	1.397	1.363 (19)
C5-N16	1.418	1.426	1.415	1.425	1.456 (3)
C6-H10	1.076	1.085	1.076	1.085	0.930
N16-H17	1.001	1.016	0.999	1.015	0.820 (4)
N16-H19	1.000	1.015	1.000	1.016	0.940 (2)
Bond Angle (°)					
C2-C1-C6	119.7	119.5	119.8	119.6	119.4 (15)
C2-C1-H7	120.1	120.2	120.1	120.2	120.3 (11)
C6-C1-H7	120.2	120.3	119.6	119.7	120.3 (11)
C1-C2-C3	120.4	120.7	120.4	120.6	121.1 (2)
C1-C2-CL11	119.8	119.6	119.8	119.7	119.5 (11)
C3-C2-CL11	119.8	119.7	119.8	119.7	119.5 (11)
C2-C3-C4	119.8	119.7	119.7	120.3	119.4 (15)
C2-C3-H8	120.1	120.2	120.1	119.5	120.3 (11)
C4-C3-H8	120.1	120.3	120.1	120.3	120.3 (11)
C3-C4-C5	120.4	120.4	119.2	119.3	121.5 (2)
C3-C4-H9	119.6	119.6	119.4	125.5	120.4 (11)
C5-C4-H9	120.0	120.0	120.1	119.4	120.4 (11)
C4-C5-C6	119.3	119.3	119.2	119.3	121.5 (2)
C4-C5-N16	120.1	120.2	120.3	120.3	119.2 (3)
C6-C5-N16	120.5	120.4	120.5	120.4	119.2 (3)
C1-C6-C5	120.5	120.5	119.8	119.6	119.4 (15)
C1-C6-H10	119.4	119.4	120.1	120.2	120.3 (11)
C5-C6-H10	120.1	120.1	120.1	120.3	120.3 (11)
C5-N16-H17	112.1	112.6	112.5	112.5	109.0 (3)
C5-N16-H19	112.3	112.5	112.4	112.7	112.9 (15)
H18-N16-H19	113.3	110.4	109.2	109.1	107.0 (2)
Torsion Angle (°)					
C6-C1-C2-C3	−0.1	−0.0	0	−0.1	1.1 (4)
C6-C1-C2-CL11	179.8	180.0	179.9	179.8	−178.4 (14)
H7-C1-C2-C3	179.9	180.0	180.0	180.0	178.9
H7-C1-C2-CL11	−0.1	−0.01	−0.1	0	−1.6
C2-C1-C6-C5	−0.1	−0.2	−0.2	0	−0.3 (4)
C2-C1-C6-H10	179.7	179.6	179.7	180	−179.7 (5)
H7-C1-C6-C5	179.8	179.8	179.8	179.8	179.7 (5)
H7-C1-C6-H10	−0.3	−0.4	−0.4	−0.2	0.3 (3)
C1-C2-C3-C4	0.1	0.1	0.1	0	−0.5 (3)
C1-C2-C3-H8	−179.8	−180.0	−180	180	−178.9
CL11-C2-C3-C4	−179.8	−179.8	−179.9	−179.9	−178.4
CL11-C2-C3-H8	0.2	0.1	0.1	0.1	1.6
C2-C3-C4-C5	0.1	0.1	0.2	0.1	−0.3
C2-C3-C4-H9	−179.4	−180.0	−179.7	−179.8	179.7
H8-C3-C4-C5	−180.0	−180.0	−179.8	−179.8	179.7
H8-C3-C4-H9	0.5	0.4	0.3	0.4	0.4
C3-C4-C5-C6	−0.4	−0.3	−0.4	−0.4	−0.5
C3-C4-C5-N16	−177.6	−177.1	−177.5	−177.1	−178.7

Table 1. (continued)

Atom	4CAN		4CAM		
Connected	HF	DFT	HF	DFT	Experimental[#]
H9-C4-C5-C6	179.2	179.5	179.5	179.6	179.5
H9-C4-C5-N16	2.0	2.7	2.4	2.8	1.3
C4-C5-C6-C1	0.4	0.3	0.4	0.3	−0.5 (3)
C4-C5-C6-H10	−179.5	−179.5	−179.5	−179.8	−179.5
C4-C5-N16-H17	−32.0	−29.5	−29.7	−31.6	−29.9
C4-C5-N16-H19	−154.9	−153.1	−153.4	−155.6	−151.9
C6-C5-N16-H17	150.8	153.7	153.3	151.7	151.9
C6-C5-N16-H19	28.0	30.1	29.5	27.7	29.9

#Ref[16]

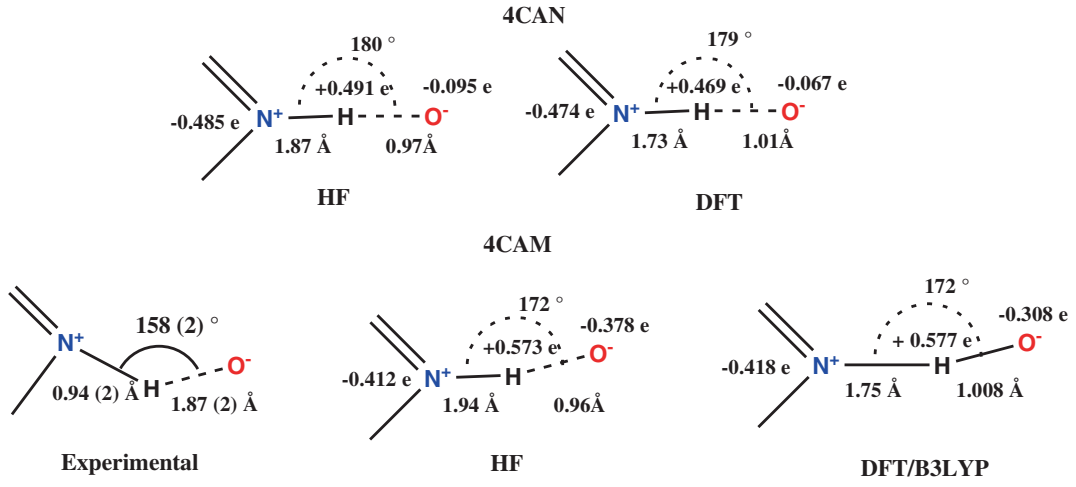

Scheme 1. Atomic charges and molecular geometry parameters calculated from experimental and theoretical calculations of the N–H· · · O hydrogen bond.

Table 2. Comparison of optimized molecular geometrical parameters of nitrate anion.

	Nitrate Anion	
Atom Connected	HF	DFT
Bond length (Å)		
N15-O12	1.189	1.222
N15-O13	1.168	1.200
N15-O14	1.318	1.379
O14-H18	0.971	1.014
Bond Angle (°)		
N15-O14-H18	107.6	106.1
O12-N15-O13	127.6	128.0
O12-N15-O14	116.9	116.9
O13-N15-O14	115.5	115.1
Torsion Angle (°)		
O14-O13-N15-O12	−179.9	−180.0
H18-O14-N15-O12	−0.4	−0.1
H18-O14-N15-O13	179.6	179.9

B3LYP levels for the molecule under study which are given in table 4 (a), 4 (b) and 4 (c) and the corresponding population analysis graph is shown in figure 3. The charge distribution of 4-chloroanilinium cation shows that the five carbon atoms attached to hydrogen atoms (C1 C3, C4, C5 and C6) are negative. Out of five carbon atoms in the 4-chloroanilinium cation, the carbon C5 atom has more negativity than the others, because the carbon (C5) atom is attached to NH_3^+ group. The elongation of C−N bond distance due to the protonation is reiterated with the electronegative repulsion between these two atoms (C5 and N16). Interestingly, another carbon (C2) atom from the cation is attached in the chlorine (Cl11) atom and both of them have electropositive charge. The characteristic feature of Cl atom is electropositive and it does not participate in any hydrogen bond. In the present case, both the methods predict that the Cl atom of the cation (Cl11) is positive (0.277 *e* in HF and 0.340 *e* in DFT) for 4CAM and (0.275 *e* in HF and 0.335 *e* in DFT) for 4CAN. This may be accorded with the formation of hydrophobic region in the crystal with the presence of the Cl atoms and the absence of N−H· · · Cl hydrogen bond.

In the 4CAM anion, all the oxygen atoms have electronegative charges. Out of four oxygen atoms, O19

Table 3. Comparison of optimized molecular geometrical parameters of maleate anion.

	Maleate Anion		
Atom Connected	HF	DFT	Experimental
	Bond Length (Å)		
C16-C17	1.488	1.481	1.476 (2)
C16-O19	1.199	1.230	1.267 (18)
C16-O20	1.302	1.321	1.234 (19)
C17-H18	1.074	1.084	0.93
C17-C23	1.326	1.343	1.325 (3)
O19-H21	1.716	1.635	1.207
H21-O25	0.954	0.990	0.930
C22-C23	1.514	1.509	1.476 (2)
C22-O25	1.307	1.33	1.267 (18)
C22-O26	1.182	1.209	1.234 (19)
C23-H24	1.075	1.085	0.93
	Bond Angle (°)		
C17-C16-O19	125.5	112.1	120.5 (14)
C17-C16-O20	111.6	122.4	117.8 (14)
O19-C16-O20	122.9	113.4	121.7 (14)
C16-C17-H18	113.4	128.7	114.9
C16-C17-C23	128.9	117.8	130.3 (8)
H18-C17-C23	117.7	110.3	114.9
C16-O19-H21	111.4	109.4	115.4
H9-O20-C16	110.7	169.6	111.2
C23-C22-O25	120.7	120.3	120.5 (14)
C23-C22-O26	117.2	117.8	117.8 (14)
O25-C22-O26	122.1	121.9	121.7 (14)
C17-C23-C22	134.2	133.8	130.3 (8)
C17-C23-H24	116.6	116.7	114.9
C22-C23-H24	109.2	109.6	114.9
H21-O25-C22	113.4	111.8	115.4
	Torsion Angle (°)		
O19-C16-C17-H18	−179.2	−179.9	179.9
O19-C16-C17-C23	0.8	0.2	0.04 (18)
O20-C16-C17-H18	0.8	0.1	0.2
O20-C16-C17-C23	−179.2	−179.9	−179.8 (9)
C17-C16-O19-H21	−0.8	0.4	−0.2
O20-C16-O19-H21	179.2	179.6	179.6
C16-C17-C23-C22	0.2	0.1	0.0
C16-C17-C23-H24	180	180	180
H18-C17-C23-C22	−179.8	−179.7	−180.0
H18-C17-C23-H24	0	−0.4	0
O25-C22-C23-C17	−0.7	−0.3	0.04 (18)
O25-C22-C23-H24	179.5	179.8	179.9
O26-C22-C23-C17	179.3	179.7	179.8
O26-C22-C23-H24	−0.6	−0.2	−0.2
C23-C22-O25-H21	0.2	0.1	0.2
O26-C22-O25-H21	−179.9	−179.9	−179.6

(–0.435 *e* in HF and 0.332 *e* in DFT) and O25 (–0.387 *e* in HF and –0.274 *e* in DFT) have more electronegativity than the others. These two oxygen atoms behave as a donor and acceptor in the O–H· · · O intramolecular hydrogen bond and these intramolecular hydrogen bonds are also observed in single-crystal XRD.

The hydrogen atom in the 4CAN anion has more electropositive charges (0.491*e* in HF and 0.469 *e* in DFT) because it is surrounded by two electronegative atoms, viz., nitrogen (N16) and oxygen (O14). This hydrogen atom plays a key role in the solid state through the N–H· · · O intermolecular hydrogen bond.

Table 4. (a) Atomic charges for optimized geometry of 4-chloroanilinium cation.

	4-chloroanilinium cation			
	4CAN		4CAM	
Atom	HF	DFT	HF	DFT
C1	−0.497	−0.507	−0.345	−0.397
C2	0.468	0.606	0.482	0.623
C3	−0.292	−0.404	−0.465	−0.533
C4	−0.109	−0.132	−0.588	−0.493
C5	−0.494	−0.398	−0.595	−0.459
C6	−0.370	−0.327	0.180	0.062
H7	0.234	0.186	0.236	0.189
H8	0.237	0.186	0.233	0.185
H9	0.205	0.159	0.187	0.148
H10	0.190	0.151	0.202	0.151
Cl11	0.275	0.335	0.277	0.340
N16	−0.485	−0.474	−0.412	−0.418
H17	0.292	0.292	0.283	0.269
H19	0.287	0.275	0.310	0.313

Table 4. (b) Atomic charges for optimized geometry of nitrate anion.

Atom	HF	DFT
O12	−0.117	−0.047
O13	−0.060	0.009
O14	−0.095	−0.067
N15	−0.159	−0.311
H18	0.491	0.469

Table 4. (c) Atomic charges for optimized geometry of maleate anion.

Atom	HF	DFT
H18	0.573	0.577
C23	−0.188	−0.310
C24	0.265	0.333
H25	0.287	0.248
O22	−0.435	−0.332
O20	−0.378	−0.308
H21	0.421	0.360
C12	0.049	−0.070
C26	−0.134	−0.174
H27	0.269	0.231
O14	−0.387	−0.274
O13	−0.327	−0.261

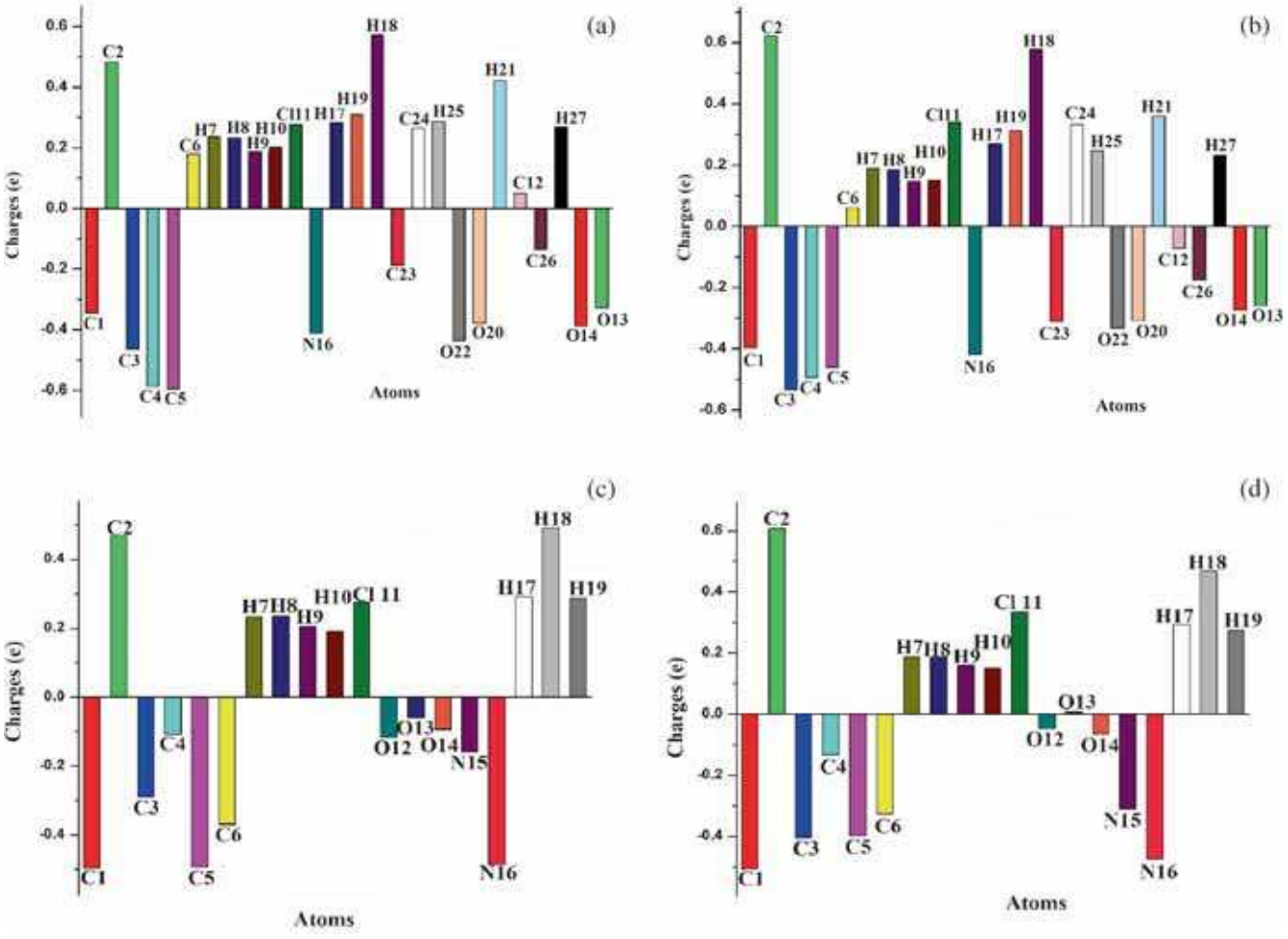

Figure 3. The atomic charges plots by HF (a) and DFT; (b) methods for 4CAM and HF; (c) DFT; (d) methods for 4CAN.

3.3 *Vibrational Analysis*

Vibrational spectroscopy can give valuable information about the hydrogen bonding forces and strength of the intermolecular bonds in addition to symmetry of the individual species. The effect of hydrogen bond is very important in crystal environment. The strong, normal and weak hydrogen bonds cause red shifting of stretching mode vibrations and blue shifting of deformation mode vibrations with different wave numbers depending on their strength. Normally, the vibrational shifts of the stretching modes are greater than that of the deformation modes. This indicates that the linear distortion is much greater than the angular distortion.

The molecular structures of 4CAM and 4CAN have various functional groups such as $-NH_3^+$, -CH, -C-N, -C-C-, -OH, -C=O, disubstituted benzene ring, etc. The vibrational bands of these groups are expected to change in their intensity and position due to their environments.[18] Complete vibrational analyses of the 72 fundamental modes of 4CAM and 51 fundamental modes of 4CAN are attempted and predicted by the quantum chemical calculations and compared with their experimental vibrational spectra. The optimized structural parameters are used in the calculation of vibrational frequencies to characterize all stationary points as minimum. The calculated vibrational wave numbers, measured by FT-IR and FT-Raman band positions with their corresponding assignments for the molecules 4CAM and 4CAN, are tabulated in tables 5 and 6, respectively. The FT-IR and FT-Raman spectra of the compounds are shown in figures 4 and 5, respectively.

3.3a *N–H Vibrations*: In general, the N–H stretching vibrations from the primary amines occur in the region 3600–3300 cm^{-1}.[19,20] In the present case, 4-choloanilinium cation has more intense peak calculated at 3588 cm^{-1} and 3504 cm^{-1} in B3LYP level to assign the NH_2 asymmetric and symmetric stretching modes, respectively, for the molecules 4CAN. Similarly, the asymmetric and symmetric $-NH_2$ stretching occurred as the less-intense peak at 3586 and 3499 cm^{-1} for the molecule 4CAM. In 4CAN, the medium band observed

Table 5. Experimental, HF and B3LYP levels computed vibrational frequencies (cm^{-1}) obtained for 4-CAN.

	Experimental		HF/6-311++G(d,p)			B3LYP/6-311++G(d,p)			
Mode Number	FT-IR	Raman	ν_{cal}	$^{a}I^{IR}$	^{b}I Raman	ν_{cal}	$^{a}I^{IR}$	^{b}I Raman	Assignment
1			15	1.9	1.2	18	1.9	2	Lattice Vibration
2			30	1.3	5.2	29	1.3	5.7	Lattice Vibration
3			37	0.1	3.8	37	0.2	4.5	Lattice Vibration
4			82	0.3	0.5	79	0.2	1	Lattice Vibration
5			91	2	1.5	99	0.7	1.2	Lattice Vibration
6			120	7.7	0.4	118	6.9	0.1	ω NH_2 + γ C-H
7			199	14.5	1.3	216	37.8	2.4	ω NH_2 + γ C-H
8			275	0.8	0.5	258	0.8	0.4	ρ NH_2 + β C-H
9			363	2	0.6	337	5	0.3	ω NH_2 + γ C-H
10			393	9.3	0.6	377	3.5	2	ρ NH_2 + β C-H
11			411	3.1	10.2	384	3.4	7.8	β (C-H + NH_2)
12			454	0.1	0.2	420	0.1	0.1	γ C-H
13			477	4.6	0.2	465	3.2	0.2	t NH_2
14			564	40.6	0.5	515	33.5	0.5	γ C-H
15			690	39.3	1.8	644	61.6	2.3	β (C-H + NH_2)
16			696	0.3	6.1	649	0.4	6.3	β C-H
17			733	5.1	2.9	653	0.5	4.1	δ O-N-O
18			777	7.1	0.3	688	4	4.8	ν N=O +δ O-N-O
19	733 w	734 w	799	15.2	2.4	718	6.9	0.7	ω NH_2 + γ C-H
20			859	14.9	11.4	787	10.4	0.3	γ O-N-O +ω NH_2 + γ C-H
21			892	4.1	18.4	813	45.1	3.8	ω NH_2 + γ C-H
22	821 m	802 m	917	39.6	0.3	822	2.9	1.4	γ C-H
23			922	1.2	0.5	829	19.5	17.9	γ C-H
24			951	81.4	0.5	904	292.5	18.1	ω NH_2 + γ O-H
25			1024	399.3	13.8	945	160.5	11.3	t CH-CH +ν N=O
26			1064	16.3	0.6	953	9.2	0.5	t CH-CH
27			1088	0.3	0.1	968	1.2	0.1	t CH-CH
28	1014 w		1102	36.9	0.9	1026	19.3	13.1	β C-H +γ O-H
29	1042 w	1047 m	1155	95.8	14.4	1032	197.5	12.1	ω NH_2 + β O-H
30	1095 m	1094 w	1160	3.7	0.9	1104	50.4	29.8	β C-H
31	1113 w		1192	5.8	0.5	1107	7.7	1.7	ρ NH_2 + β C-H
32	1149 w	1175 m	1197	46.1	20.7	1156	6.5	1.1	ρ NH_2 + β C-H
33	1202 w	1209 w	1289	6.7	3.2	1201	6.5	5.1	β C-H
34			1317	0.4	1.2	1261	118.8	22.2	ν C-N +β C-H
35			1354	79.6	16.2	1319	4.1	2.2	β C-H
36			1449	0.6	0.7	1328	279.5	25.4	ν N=O
37			1567	233.1	6.2	1350	1.2	0.5	ρ NH2 +β C-H
38			1573	4	0.6	1458	3.3	0.1	ρ NH2 +β C-H
39	1489 m		1611	569.6	10.9	1497	395	5	β O-H
40	1542 m	1535 w	1657	126.6	1.3	1525	111.2	1	β C-H
41		1601 m	1772	2.1	4.6	1628	2.6	3	ρ NH_2 + ν C-C +β C-H
42			1785	12.1	23.2	1641	8.7	54.7	δ NH_2 + ν C-C +β C-H
43			1806	79.8	24.4	1661	63.1	14.6	δ NH_2
44	1752 m		1928	626.4	2.9	1734	280	3.5	ν N=O +β O-H
45		3078 w	3324	11.5	71.2	2907	2497.3	364.1	ν N-H$\cdots$O
46			3332	5.5	60.4	3167	8.6	82	ν C-H
47			3362	3.4	48.7	3172	5.5	67.6	ν C-H
48			3364	0.5	142.8	3203	1.5	38.1	ν_{as} C-H
49			3595	1529.6	158.5	3204	0.1	177.3	ν_sC-H
50			3742	36.5	113.1	3504	24.3	165.6	ν_s NH_2
51			3826	26.4	41.2	3588	24.9	46.4	ν_{as} NH_2

w – weak; vs – very strong; m – medium;
ν, Stretching; ν_s, sym.stretching; ν_{as}, asym.stretching; β – in-plane bending; γ – out-of-plane bending; ω – Wagging;
t – twisting; δ – Scissoring; ρ – Rocking;

Table 6. Experimental, HF and B3LYP levels computed vibrational frequencies (cm^{-1}) obtained for 4-CAM.

	Experimental		HF/6-311++G(d,p)			B3LYP/6-311++G(d,p)			
Mode Number	FT-IR	Raman	ν_{cal}	[a]I^{IR}	[b]I Raman	ν_{cal}	[a]I^{IR}	[b]I Raman	Assignment
1			8	1.8	1.9	6	1.8	2.5	Lattice Vibration
2			24	3.6	2.8	26	2.7	3.8	Lattice Vibration
3			27	2.3	3.3	30	3.2	3.3	Lattice Vibration
4			30	0.9	1.6	35	0.1	3.4	Lattice Vibration
5			58	4.1	1.2	64	4.4	1	Lattice Vibration
6			76	6.7	0.1	78	7.4	0.1	β (C-H + O-H)
7			87	1.2	0.6	90	1.3	0.7	β (C-H + O-H)
8			103	4.7	2	107	5.2	1.6	γ C-H +β (C-H + O-H)
9			181	5.1	2.2	192	13	4.4	ω NH_2
10			250	31	0.5	256	19.6	0.6	ρ NH_2
11			276	0.3	0.4	260	35.6	0.5	ρ NH_2 + β O-H
12			304	11.7	1.9	297	3.8	2.8	t CH-CH
13			331	3	5.2	299	12.3	1.9	β (C-H + O-H)
14			363	1.9	0.8	338	4.7	0.5	ω NH_2 + γ C-H
15			389	10	0.5	377	6	2	ρ NH_2 + β C-H
16			411	3.1	9.3	384	4.4	6.3	ρ NH_2 + β C-H
17			433	4.8	4.6	409	22.9	6.5	ρ NH_2 + β O-H
18			455	0.2	0.2	420	0.5	0.1	t CH-CH
19	489 m		475	1.2	0.5	474	2	0.6	t NH_2
20			567	40.9	0.6	517	30.4	0.7	ω CH-CH
21			649	10.2	1.7	593	1.6	0.7	ω CH-CH
22	569 m		653	2.8	0.9	601	11.2	2.9	β (C-H + O-H) +ω CH-CH
23		636 s	671	51.1	1.6	634	21.2	1.8	β (C-H + O-H) +ω CH-CH
24			691	43	2.4	646	51.4	1.7	β (O-H + C- NH_2)
25	694 s		697	0.3	6.2	651	0.9	5.8	Ring deformation
26			782	10.8	0.8	719	8.6	0.9	ω NH_2 + γ C-H
27			786	114.8	0.4	784	17.5	1.9	γ (C-H + O-H)
28			847	44.5	0.2	788	21.2	0.5	β (C-H + O-H)
29	815 w	806 s	867	29.8	12.7	815	55.8	3.3	ω NH_2 + γ C-H
30			881	2.4	8.4	823	4.3	2.8	ω CH-CH
31			900	15	16.3	830	11.5	20.3	ω NH_2 + γ C-H
32			913	2.3	8.5	834	101.5	1.1	γ O-H
33			922	0.3	0.8	850	1.4	9.4	β (C-H + O-H)
34	877 m		964	53	1.2	875	25	0.8	ω CH-CH
35		904 w	973	155.2	1.6	905	339	25.2	ω NH_2 + γ C-H
36			1025	354	13.5	954	13.1	1.6	t CH-CH
37			1028	33.8	2.4	956	36.7	3	ρ CH-CH +β O-H
38			1065	6.6	0.3	970	2.6	0.2	t CH-CH
39	999 w	1013 w	1089	0.3	0.1	1028	23.8	2.1	ρ CH-CH
40			1101	31.5	1.2	1031	0.2	3.1	t CH-CH (Maleate)
41	1089 w	1094 m	1139	0.1	7.2	1086	122.3	16.2	ρ NH_2 + γ O-H
42			1160	4.1	0.8	1104	50.4	31.6	β C-H
43			1191	6.4	0.5	1110	22.3	5	ρ NH2 +β C-H
44	1176 w	1183 w	1197	46.3	21.1	1156	7.8	1	ρ NH2+β C-H
45	1213 w	1208 w	1289	7.6	3.3	1201	6.6	5.5	δ CH-CH
46			1316	3	0.7	1219	90.7	12.6	β C-H (Maleate)
47		1242 w	1326	85.8	13.3	1262	174.1	33.3	ν C-N +β C-H +ω NH_2
48			1357	109.1	17.7	1288	327.3	16.7	ν C-O+β (C-H+ O-H) (Maleate)
49			1395	407.1	3.4	1317	40.3	21.8	β (C-H + O-H) (Maleate)
50			1432	44.9	18.7	1319	5.5	1	β C-H
51	1394 w	1394 s	1449	0.1	0.8	1350	1.8	0.5	ρ NH_2 + β C-H
52			1511	12.8	5.2	1416	52.1	18.7	β (C-H + O-H) (Maleate)
53	1460 m		1558	297.3	3.7	1457	94.4	0.9	β (C-H + O-H)
54			1573	13.1	0.3	1459	111.9	0.5	β (C-H + O-H) +ρ NH_2
55			1590	147.1	3.7	1492	84.8	9.3	β (O-H + C-H) (Maleate)
56	1579 m		1657	153.4	1.2	1525	149.3	1	β C-H
57		1616 m	1771	2.9	5	1628	3.3	5.7	C-H sextant +ρ NH_2
58			1785	12	28.1	1641	20.2	64.3	β C-H +δ NH_2
59			1807	87.7	23.2	1663	74.2	13	δ NH_2

Table 6. (continued)

Mode Number	Experimental		HF/6-311++G(d,p)			B3LYP/6-311++G(d,p)			Assignment
	FT-IR	Raman	ν_{cal}	$^{a}I^{IR}$	^{b}I Raman	ν_{cal}	$^{a}I^{IR}$	^{b}I Raman	
60		1685 m	1850	192.6	159.1	1680	117.6	201.6	ν C=C +β O-H
61			1918	405.4	39.1	1706	323.1	45	ν C=O +β (C-H +O-H)
62			2003	497.3	95.2	1786	319.1	111.4	ν C=O +β (C-H +O-H)
63	3041 w	3043 s	3324	11.7	71.1	2971	3159.4	628.1	ν N-H$\cdots$O
64		3082 s	3332	6.3	65.3	3167	8.6	82	ν C-H
65			3343	0.1	42.5	3172	5.9	71.7	ν_{as} CH-CH
66			3362	3.9	51.8	3173	0.3	41.9	ν_{as} CH-CH (Maleate)
67			3362	1	101.9	3190	1.5	131.6	ν_{s} CH-CH (Maleate)
68			3363	0.4	141.7	3203	1.5	63.6	ν_{s} C-H
69			3725	1297.9	317.1	3204	0.2	155.1	ν C-H
70			3748	358.9	88.8	3290	810.6	72.8	ν O-H..O
71			3831	30.4	43.4	3499	30.5	172.9	ν_{s} NH_2
72			3872	582.4	35.4	3586	26.8	52	ν_{as} NH_2

w – weak; vs – very strong; m – medium;
ν, Stretching; ν_s, sym.stretching; ν_{as}, asym.stretching; β – in-plane bending; γ – out-of- plane bending; ω – Wagging; t – twisting;
δ– Scissoring; ρ – Rocking

at 3078 cm^{-1} in Raman spectrum is assigned to the N–H stretching. This stretching vibration was calculated as a very strong band at 3324 and 2907 cm^{-1} in HF and B3LYP level. In 4CAM, the same stretching vibration is

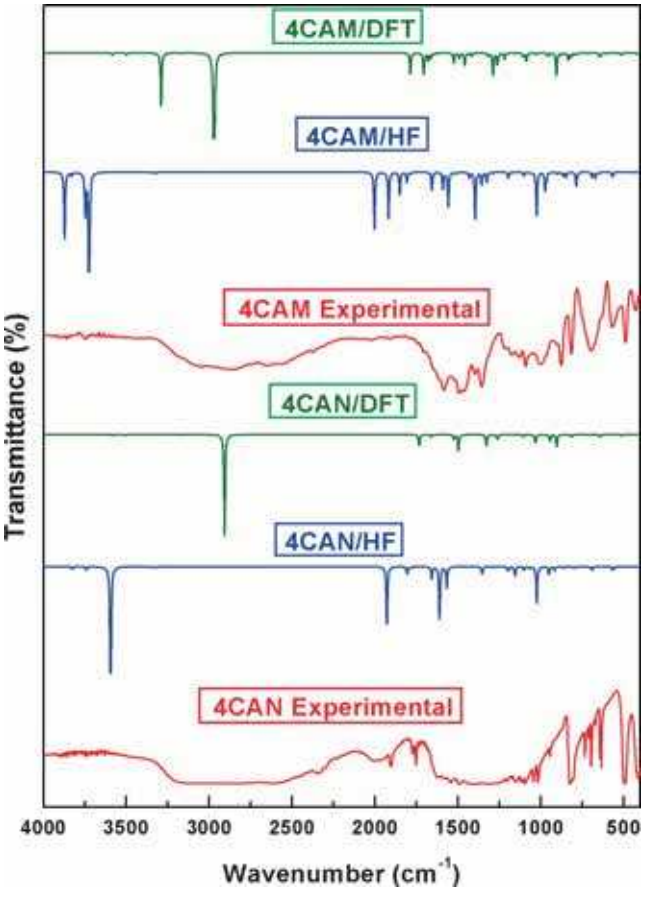

Figure 4. Comparative representation of FT-IR spectra of 4CAM and 4CAN.

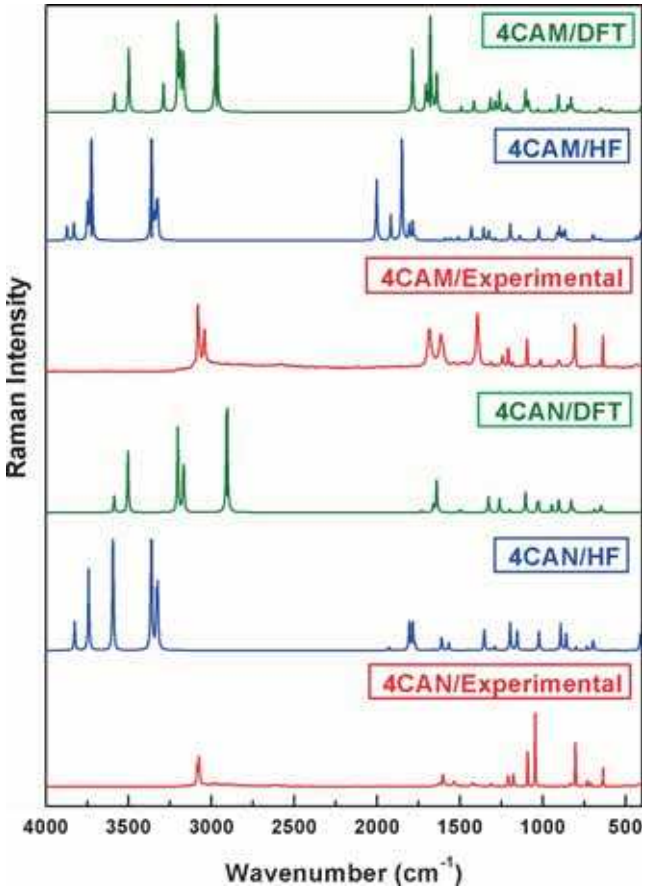

Figure 5. Comparative representation of FT-Raman spectra of 4CAM and 4CAN.

observed as a weak band at 3041 cm^{-1} in IR spectrum and strong band at 3043 cm^{-1} in Raman spectrum. This corresponding vibration is calculated at 3324 and 2971 cm^{-1} in HF and B3LYP methods, respectively. These calculated stretching vibrations are occurred as a very strong peak in theoretical methods due to the N–H$\cdots$O hydrogen bond. But, in the case of experimental IR spectra, the N–H$\cdots$O hydrogen bond trace is observed as a very broad spectrum around 3200–2200 cm^{-1} for both the molecules. The occurrences of sharp and broad peaks of the spectrum in the theoretical and experimental methods are due to the fact that the theoretical calculations are carried out in isolated gas state whereas the crystalline state is dominated with the excessive hydrogen bonding interactions. As the hydrogen atom is placed between two heavier electronegative atoms (donor and acceptor) the resulted vibration is observed at a very strong intensity peak for the N–H$\cdots$O band in theoretical computation. It confirms the relocation of proton from the acids to amino group.

The scissoring vibration of the amine group appears at 1630–1610 cm^{-1}. As one of the H atoms of the amine group is strongly involved in the N–H$\cdots$O intermolecular interactions between ion pairs, the NH_3^+ group vibration is reduced to –NH_2molecular vibration. In molecule 4CAN, $NH_2$of NH_3^+ scissoring vibration was calculated at 1661 and 1641 cm^{-1} in DFT/B3LYP method. The vibration coincides with 4CAM at 1663 cm^{-1}. In both the molecules, the HF level is more deviated from the DFT level. The vibrational mode mentioned above is not observed in the experimental spectra. In 4CAN, the medium band at 1601 cm^{-1} in Raman spectrum is assigned to the NH_2 rocking vibration and the corresponding vibration is predicted at 1772 and 1628 cm^{-1} in HF and B3LYP method, respectively. In lower wavenumber regions, most of the bands are observed in the scissoring, rocking and wagging vibrations. It is in good agreement with the experimental results.

3.3b *C–H, C–C and C–N vibrations*: The aromatic C–H stretching vibrations are observed in the region 3100–3000 cm^{-1}.[21] This is the characteristic region for identification of the C–H stretching vibrations. Also, the bands are not affected appreciably by the nature of the substituents in this region. The asymmetric C–H stretching is calculated at 3595 and 3204 cm^{-1} in HF and DFT/B3LYP methods, respectively for 4CAN. In 4CAM, the same vibration is observed at 3725 and 3204 cm^{-1} in HF and DFT/B3LYP methods respectively. The C–H symmetric stretching vibration is predicted at 3364 cm^{-1} in HF level and 3203 cm^{-1} in DFT/B3LYP method for 4CAN and 3363 cm^{-1} in HF and 3203 cm^{-1} in DFT/B3LYP methods for 4CAM. These asymmetric stretching vibrations are not observed in the experimental results. In 4CAM, the strong peak observed at 3082 cm^{-1} in Raman spectrum is assigned to the C–H stretching vibration; this stretching vibration is computed at 3332 cm^{-1} in the HF level and at 3167 cm^{-1} in the B3LYP level.

The substituted benzene ring has six C–C stretching vibrations. These vibrations mainly involve 'quadrant stretching' of the phenyl C–C bonds. But there is a small interaction with C–H in-plane bending vibration. There are two quadrant-stretching components in substituted benzenes are expected to appear in the regions 1620–1585 and 1590–1565 cm^{-1}, respectively. The 1600 cm^{-1} doublet region is not frequency sensitive to the nature of substitution at ortho, meta and para positions. For these types of substitutions, the quadrant stretching vibrations are infrared inactive because all atoms from the ring are moving to the opposite directions. The C–C stretching vibrations mixed with NH_2 deformation modes and observed in the modes of 41 and 42 for 4CAN molecule and 57 for 4CAM molecule. In 4CAM, the weak band at 1242 cm^{-1} in Raman spectrum and IR inactive is assigned to the C$-$N stretching mode. These modes are mixed with C–H in-plane deformation modes. The same vibration is computed at 1326 and 1262 cm^{-1} in the HF and B3LYP methods respectively. It is matched well with the 4CAN molecule.

In general, free O–H stretching vibrations appeared around 3600 cm^{-1}.[22] In the present case, the intense band is computed at 3748 cm^{-1} and 3290 cm^{-1} in the HF and DFT/B3LYP methods respectively (table 5). These results show that the DFT/B3LYP method gets downshifted to the literature value which is due to the strong O–H$\cdots$O intramolecular interaction in the maleate anion. It confirms the migration of the proton transfer between the two O atoms of the anion. The O–H...O stretching vibration in the intramolecular hydrogen bonds is crucial in the crystal packing. The medium band observed at 1685 cm^{-1} in Raman spectrum is assigned to O–H in-plane bending vibration. The theoretically computed frequency for O–H in-plane bending vibration by DFT/B3LYP method matches well with the experimental results. The medium band at 1460 cm^{-1} in IR spectrum is assigned to the O–H in-plane bending vibration mixed with C–H in-plane bending vibration. The O–H outof-plane bending vibration is observed at the weak band at 1089 cm^{-1} in the IR spectrum and the medium band at 1094 cm^{-1} in the Raman spectrum; this vibration is mixed with NH_2 rocking vibration. In lower wavenumber regions most of the bands assigned to the O–H in-plane bending vibrations are mixed with the C–H in-plane bending vibration.

3.3c *O–H Vibrations of Maleate Anion*:

3.3d *Vibrations of the Nitrate Anion*: In the free state the nitrate group has D_{3h} symmetry and its normal modes of vibrations are A_1' (ν_1), $A_2''(\nu_2)$ and $E'(\nu_3$ and $\nu_4)$. In which, ν_1 is Raman active, $\nu_2$is IR active, ν_3 and $\nu_4$are both IR and Raman active. In the free state of the NO_3^- anion, the symmetric stretching vibration occurs at 1049 cm^{-1} the symmetric bending vibration appears at 530 cm^{-1} and ν_3 and ν_4 (asymmetric stretching and bending modes) occur at 1355 and 690 cm^{-1}, respectively.[23–25]

The medium band at 1752 cm^{-1} in IR spectrum is assigned to the N=O stretching vibration. The same vibration is computed at 1928 and 1449 cm^{-1} in HF and 1734 and 1328 cm^{-1} in DFT/B3LYP methods respectively (table 6). The weak band at 1042 cm^{-1} in IR spectrum and medium band at 1047 cm^{-1} in Raman spectrum is assigned to the N–O in-plane bending vibration. The corresponding vibration is computed at 1155 and 1032 cm^{-1} in the HF and DFT/B3LYP methods respectively. The out-of-plane deformation is observed at 859 (HF) and 787 cm^{-1} (DFT/B3LYP) method. These deformation modes are mixed with the NH_2 wagging vibration. These results show migration of proton transfer between the cation and nitrate group of the anion. This out-of-plane deformation is not present in the experimental results.

3.4 *NBO Analysis*

In the NBO analysis, the electronic structures are explained in terms of a set of occupied Lewis and a set of non-Lewis localized orbitals.[26] Also, delocalization effects can be identified by the presence of off-diagonal elements of the Fock matrix in the NBO basis. The NBO method gives information about interactions in both filled and virtual orbital spaces that could enhance the analysis of intra- and intermolecular interactions.

The delocalization effects of the present molecules can be identified by the diagonal elements of the Fock matrix in the NBO basis. The strengths of these delocalization interactions, $E^{(2)}$, are estimated by second-order perturbation theory. The second-order Fock matrix was calculated to evaluate the donor–acceptor interactions.[27] These interactions result in loss of occupancy from the localized NBO of the idealized Lewis structure into an empty non-Lewis orbital. For each donor (i) and acceptor (j), the stabilization energy $E^{(2)}$ associated with the delocalization $i \rightarrow j$ is estimated as

$$E^{(2)} = q_i \frac{F(i,j)^2}{(\varepsilon_j - \varepsilon_i)} \quad (1)$$

where q_i is the donor orbital occupancy, ε_i and ε_j are the orbital energies and $F(i, j)$ is an off- diagonal NBO Fock matrix element. NBO analysis provides an efficient method for studying intra- and intermolecular bonding and interaction among bonds and also provides a convenient basis for investigating charge transfer or conjugative interaction in molecular systems. Some electron donor orbital, acceptor orbital and the interacting stabilization energy resulting from the second-order micro-disturbance theory are reported.[28,29]

NBO analyses of both the molecules have been carried out by the B3LYP/HF method with 6-311++ G(d,p) basis set, in order to explain the intramolecular, re-hybridization and delocalization of electron density within the molecules. In the NBO analysis of the hydrogen bonded systems, the most significant element is the charge transfer between the lone pairs of the proton acceptor and the anti-bonds of the proton donor. In case of the present molecular structures, intramolecular charge transfer leads to C–C bond in the aromatic ring. As a result of this intramolecular charge transfer, the aromatic ring of the molecules is stabilized, which is due to the N–H$\cdots$O intermolecular hydrogen bonds. The interaction between bonding and anti-bonding of C–C bond has large stabilization energy due to the hyperconjugative interactions of π (C–C) $\rightarrow$ π^* (C–C). The intermolecular hyperconjugative interactions π (C1–C2) $\rightarrow$ π^* (C3–C4) lead to stabilization of 39.47 kJ/mol in HF and 19.45 kJ/mol in DFT method for 4CAN and 38.46 kJ/mol in HF and 18.52 kJ/mol in DFT method for 4CAM. This interaction enhances further conjugation with anti-bonding orbital of π^*(C5–C6), which leads to strong delocalization energies for both the molecules. The same kind of interaction was identified as π (C3–C4), which is presented in tables TS1 and TS2 (supplementary material) for both the molecules. The lone pair chlorine atom in both molecules has the highest occupancies and the stabilization energies also increase. But in the present case, the chlorine atom does not participate in any intermolecular hydrogen bonds because the chlorine atom has an electropositive charge. Much of the delocalization takes place in the aromatic ring, which is due to the proton transfer between the cation and anion. This larger delocalization of the 4-chloroaninline cation stimulates the bioactivity nature.

3.5 *HOMO and LUMO analysis*

In general, the highest occupied molecular orbital (HOMO) and lowest unoccupied molecular orbital (LUMO) are called as frontier molecular orbitals. These orbitals give information about the chemical hardness,

electro-negativity and chemical potential of the molecule.[30] The HOMO and LUMO energies of the molecules 4CAM and 4CAN were calculated by the B3LYP/HF methods with basis set of 6-311++ G(d,p) as listed in table TS3 (supplementary material). The corresponding energy level diagrams are shown in figures 6 and 7, respectively. From these figures, it is observed that the energy levels 320 and 429 in 4CAM and 4CAN are in the energy ranges of -104.843 a.u. to 219.354 a.u. and -101.563 a.u. to 215.760 a.u. in HF and DFT method, respectively, for both molecules. The energy difference between HOMO and LUMO analyses is called as energy gap, which is an important feature for stability of the structures. The calculated energy values of LUMO and HOMO are 0.027 a.u. and -0.328 a.u. for 4CAM at the HF level and -0.109 a.u. and -0.250 a.u. by the DFT method, -0.028 a.u. and - 0.330 a.u. at the HF level, -0.079 a.u. and -0.250 a.u. in DFT level for 4CAN. The frontier molecular orbital energy gap value of 4CAM molecule is 0.355 a.u. at the HF and 0.141 a.u. at the DFT level and the same energy gap of 4CAN is 0.358 a.u./ 0.171 a.u. in the HF/B3LYP method. The results show that the molecules are having a small frontier energy gap. This small energy gap is associated with a high chemical reactivity, because a huge amount of

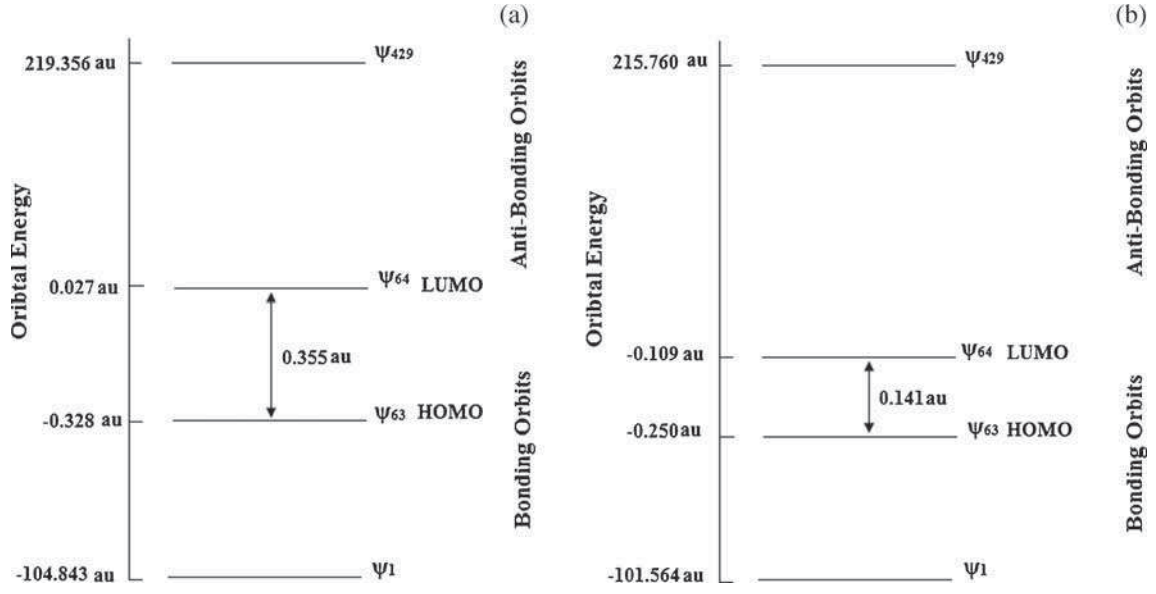

Figure 6. Energy level diagram of molecular orbits of 4CAM by (a) HF and; (b) B3LYP levels.

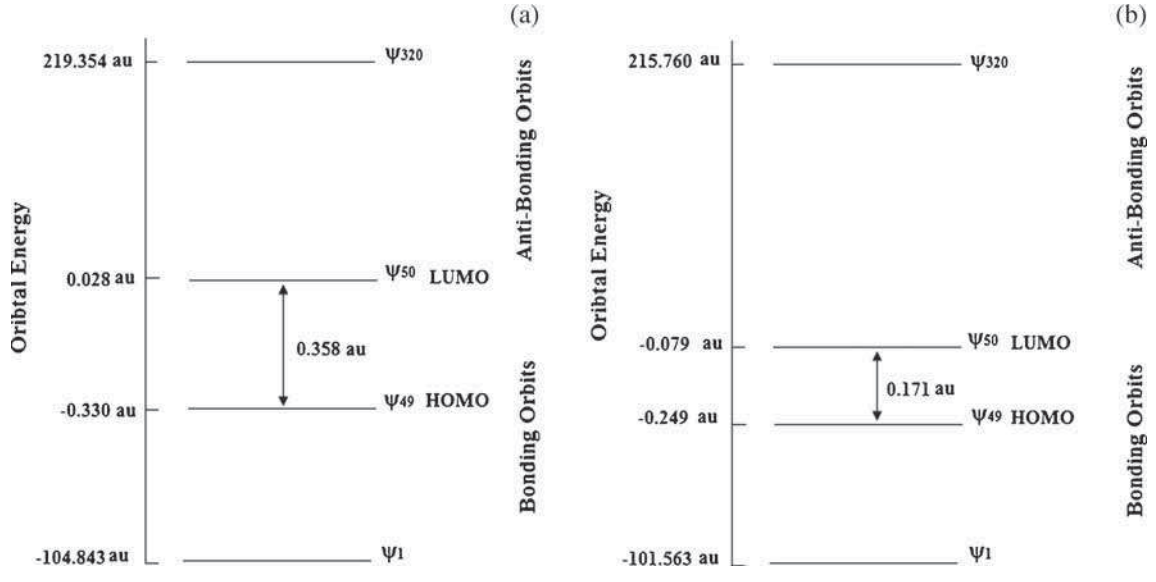

Figure 7. Energy level diagram of molecular orbits of 4CAN by (a) HF and; (b) B3LYP levels.

charge transfer occurs within the molecule. The narrow energy gap between HOMO and LUMO supports the possible bioactivity of the molecule.

4. Conclusions

The experimental and theoretical investigations reveal the proton transfer between the 4-chloroanilinium cation and maleate and nitrate anions. This proton transfer provides the support for the molecular assemblies dominated by the strong inter and intramolecular N–H$\cdots$O and O–H$\cdots$O hydrogen bonds. The optimized molecular structure, vibrational frequencies and NBO analysis of 4-chloroanilinium salts were found out by quantum chemical calculations at the HF and DFT/B3LYP methods invoking 6-311++G(d,p) basis sets. The shifting of vibrational bands due to the intermolecular hydrogen bonds was analyzed with experimental and theoretically computed vibrational spectra. Natural bond orbital analysis indicates the strong intermolecular interactions and in an agreement with the experimental intermolecular hydrogen bonding results. Natural bond orbital analysis of the molecule confirms that the charge transfer caused by π electron cloud movement from donor to acceptor must be responsible for the bioactivity. The value of the energy gap between the HOMO and LUMO gived the information about chemical softness, chemical hardness, electronegativity and chemical potential of the molecules.

Supplementary Information

X-ray crystallography data of the compound, 4CAM, is available in Cambridge Structural Database (CSD), Ref No: 877151.

Acknowledgement

The authors SA and SSK thank the Department of Science and Technology, SERB for the financial support of this work in the form of Fasttrack Research Project scheme.

References

1. Deechongkit S, Nguyen H, Powers E T, Dawson P E, Gruebele M and Kelly J W 2004 *Nature* **430** 101
2. Lopez N, Vos T E, Arif A M, Shum W W, Noveron J S and Miller J S 2006 *Inorg. Chem.* **45** 4325
3. Senes A, Ubarretxena-Belandia I and Engelman D M 1998 *Proc. Natl. Acad. Sci.* USA p. 9056
4. Parker L L, Houk A R and Jensen J H 2006 *J. Am. Chem. Soc.* **128** 9863
5. Aakeroy C B and Seddon K R 1993 *Chem. Soc. Rev.* **22** 397
6. Desiraju G R 1989 In *Crystal Engineering: The Design of Organic Solids* (Amsterdam: Elsevier)
7. Harms K and Wocadlo S 1995 In *XCAD4* (Germany: University of Marburg)
8. Sheldrick G M 2008 *Acta Cryst. A* **64** 112
9. Farrugia L J 1997 *J. Appl. Cryst.* **30** 565
10. Macrae C F, Edgington P R, McCabe P, Pidcock E, Shields G P, Taylor R, Towler M and Van de Streek J 2006 *J. Appl. Cryst.* **39** 453
11. Frisch M J, Trucks G W, Schlegel H B, Scuseria G E, Robb M A, Cheeseman J R, Scalmani G, Barone V, Mennucci B, Petersson G A, Nakatsuji H, Caricato M, Li X, Hratchian H P, Izmaylov A F, Bloino J, Zheng G, Sonnenberg J L, Hada M, Ehara M, Toyota K, Fukuda R, Hasegawa J, Ishida M, Nakajima T, Honda Y, Kitao O, Nakai H, Vreven T, Montgomery J A, Peralta J E, Ogliaro F, Bearpark M, Heyd J J, Brothers E, Kudin K N, Staroverov V N, Kobayashi R, Normand J, Raghavachari K, Rendell A, Burant J C, Iyengar S S, Tomasi J, Cossi M, Rega N, Millam J M, Klene M, Knox J E, Cross J B, Bakken V, Adamo C, Jaramillo J, Gomperts R, Stratmann R E, Yazyev O, Austin A J, Cammi R, Pomelli C, Ochterski J W, Martin R L, Morokuma K, Zakrzewski V G, Voth G A, Salvador P, Dannenberg J J, Dapprich S, Daniels A D, Farkas O, Foresman J B, Ortiz J V, Cioslowski J and Fox D J 2013 *Gaussian 09, Revision A.1, Gaussian, Inc.*, Wallingford CT
12. Schlegel H B 1982 *J. Comput. Chem.* **3** 214
13. Hohenberg P and Kohn W 1964 *Phys. Rev. B.* **136** 864
14. Becke A D 1993 *J. Chem. Phys.* **98** 5648
15. Dennington R, Keith T and Millam J 2009 *J. Semichem Inc.*, Shawnee Mission KS
16. Anitha R, Athimoolam S, Asath Bahadur S and Gunasekaran M 2012 *Acta Cryst. E* **68** o959
17. Sidir I, Sidir Y G, Kumalar M and Tasal E 2010 *J. Mol. Struct.* **964** 134
18. Ploug-Sørensen G and Andersen E K 1983 *Acta Cryst. C* **39** 112
19. Kurt M, Yurdakul M and Yurdakul S 2004 *J. Mol. Struct. (Theochem.)* **711** 25
20. Krishnakumar V and John Xavier R 2005 *Spectrochim. Acta Part A* **61** 253
21. Socrates G 1980 In *Infrared Characteristics Group Frequencies* (New York: John Wiley)
22. Lampert H, Mikenda W and Karpten A 1997 *J. Phys. Chem. A* **101** 2254
23. Banwell C N and Mccash E M 1995 In *Fundamentals of Molecular Spectroscopy* 4th ed. (New Delhi: Tata McGraw Hill)
24. Dollish F R, Fateley W G and Bentley F F 1973 In *Characteristic Raman Frequencies of Organic-Compounds* (New York: Wiley)
25. Rosenthal M R 1973 *J. Chem. Educ.* **50** 331
26. Reed A E, Curtis L A and Weinhold F A 1988 *Chem. Rev.* **88** 899

27. Szafran M, Komasa A and Adamska E B 2007 *J. Mol. Struct. (THEOCHEM)* **827** 101
28. James C, Amal Raj A, Reghunathan Joe I H and Jayakumar V S 2006 *J. Raman Spectrosc.* **37** 1381
29. Na L J, Rang C Z and Fang Y Z J 2005 *Zhejiang Univ. Sci. B* **6** 584
30. Fleming I 1976 In *Frontier Orbitals and Organic Chemical Reactions* (New York: John Wiley)